Proc. Fifth Annual Int. High Level Radioactive Waste Management Conference, 2007-19, May 22-26, Las Vegas, NV, USA

WETTING PHASE PERMEABILITY IN A PARTIALLY SATURATED HORIZONTAL FRACTURE

M.J. Nicholl and R.J. Glass
Geohydrology Division 6115
Sandia National Laboratories
Albuquerque, NM 87185

Abstract

Fractures within geologic media can dominate the hydraulic properties of the system. Therefore, conceptual models used to assess the potential for radio-nuclide migration in unsaturated fractured rock such as that composing Yucca Mountain, Nevada, must be consistent with flow processes in individual fractures. A major obstacle to the understanding and simulation of unsaturated fracture flow is the paucity of physical data on both fracture aperture structure and relative permeability. An experimental procedure is developed for collecting detailed data on aperture and phase structure from a transparent analog fracture. To facilitate understanding of basic processes and provide a basis for development of effective property models, the simplest possible rough-walled fracture is used. Stable phase structures of varying complexity are created within the horizontal analog fracture. Wetting phase permeability is measured under steady-state conditions. A process based model for wetting phase relative permeability is then explored. Contributions of the following processes to reduced wetting phase permeability under unsaturated conditions are considered: reduction in cross-sectional flow area, increased path length, localized flow restriction, and preferential occupation of large apertures by the non-wetting phase.

Introduction

Fractures within geologic media tend to dominate hydraulic behavior of the system under both saturated and unsaturated conditions, particularly when the matrix is of low permeability. When fully saturated with a flowing phase, individual fractures act as conduits through the media and allow free passage of that phase between the matrix blocks which bound the fracture. As phase saturation decreases, flow between the bounding matrix blocks and in-plane flow through the fracture are both restricted. Permeability of the fracture to in-plane flow of a given phase is a discontinuous function of phase saturation. Under steady state conditions, flow in a single phase along the plane of a fracture will be confined to the connected network of apertures filled by that phase; if lowering phase saturation breaks the continuity of that network, then in-plane flow will cease. The effects of phase saturation on fracture permeability are of significant interest to a variety of disciplines within the geo-sciences, including petroleum extraction, geothermal energy, and ground water contamination.

Exploration of two-phase fracture flow has been stimulated in recent years by the proposed geologic isolation of high-level radioactive waste in unsaturated fractured rock, such as that located at Yucca Mountain, Nevada. Performance assessment exercises to consider the possibility for off-site migration of radio-nuclides are used to evaluate the suitability of a potential repository site[1]. Numerical models used in performance assessment exercises are based on conceptual models of flow and transport through unsaturated fractured rock. Exploration of flow in individual fractures is a necessary step towards the construction of conceptual models consistent with real world flow processes.

The vast majority of recent work on two-phase flow in individual fractures has involved numerical simulation of both the aperture field and flow process; see Murphy and Thompson[2] for a concise review of previous work. Such simulation has been necessitated by a paucity of physical data regarding both spatial structure of fracture apertures and flow processes within a variable aperture field. Two-dimensional aperture fields measured at the sub-millimeter scale have only recently been published[3,4]. In addition, to our knowledge, there are no published data of pressure/saturation or relative permeability relations measured on single natural fractures. Relative permeability has been measured recently in a transparent natural fracture cast where phase saturation geometry could be observed[5].

We begin our study of fracture relative permeability with an analog rough-walled fracture that is fabricated from two sheets of textured plate glass. The resultant statistically homogeneous, transparent analog fracture eliminates the effects of matrix imbibition, aperture heterogeneity, and differential surface wettability while allowing data collection through transmitted light visualization. Gravitational effects are eliminated by orienting the analog fracture along the horizontal plane. Through use of this simplest possible rough walled fracture, we are able to develop techniques for spatial characterization of aperture and phase structure. Those techniques are then used to explore the effects of phase structure on fracture relative permeability. Use of a statistically homogeneous analog fracture eliminates macroscopic control of the phase structure by the aperture field. The techniques and understanding developed in this investigation will be applied in future studies to statistically heterogeneous aperture fields as exhibited in cast replicas of natural fractures and designed into manufactured analog fractures. Such studies are necessary to build a proper foundation for valid simplifications of fracture behavior

required in effective property models for use in the performance assessment exercises.

Here we employ optical visualization techniques to explore steady-state flow of the wetting phase through two-phase structures of varying saturation and complexity. Water is used as the wetting phase, and air as the non-wetting phase. We begin by providing a short description of the experimental apparatus, imaging system, and technique for measurement of relative permeability. A detailed description of methodologies for characterization of aperture and phase structures through use of simple light absorption theory is then presented. A course of experimentation in two-phase structures of varying complexity and saturation is described. Measurements of apertures filled by the non-wetting phase are used to compare experimental phase structures to predictions based on current conceptual models of fracture-matrix equilibrium (e.g. Wang and Narasimhan[6]). Measurements of fracture relative permeability are then presented and discussed relative to a simple process oriented model. We conclude by summarizing results and providing a short discussion of future work directed towards the development of process oriented effective property models.

We note that strong analogies can be made from the two-phase system considered in these experiments consisting of a liquid wetting phase (water) and a gaseous non-wetting phase (air) to other systems of importance. Because experiments were performed under steady-state conditions, spatial structure of the entrapped phase is invariant, acting simply to prevent wetting phase flow through the occupied regions. This scenario is directly analogous to single phase flow through fractures exhibiting significant contact area. Experimental results are also applicable to steady state flow through a stable two-phase structure of immiscible liquids, such as oil/water or more generally water/NAPL.

Experimental Approach

An analog rough-walled fracture is fabricated by holding two textured glass plates (30.5 x 15.25 cm) in close contact. Application of a confining pressure (20 psi) assures that the resultant aperture field exhibits statistical homogeneity. Flow is directed along the long axis of the analog fracture through implementation of no-flow boundaries along the fracture sides. Fluid is uniformly supplied to one end of the fracture using a pressure-stabilized peristaltic pump, creating a constant flow boundary condition. At the downstream end of the fracture, a constant head boundary is implemented, with mass flow rate measured at the outflow. Manometers located at the upstream and downstream boundaries are used to quantify differential pressure head; hydraulic conductivity (K) may then be calculated through use of Darcy's law. As fluid density and viscosity were held constant, relative permeability (k_r) may be defined as the ratio of measured K to that obtained under saturated conditions (K_s).

$$k_r = \frac{K}{K_s} \qquad (1)$$

The transparent nature of the analog fracture allows collection of wetted structure data through the use of digital imaging techniques. Hydraulic conductivity measurements were conducted with the test fracture placed on a horizontally oriented table that is back-lit with high-frequency fluorescent lamps. The imaging system focused on the fracture plane is capable of obtaining data at 2048 x 2048 pixels of spatial resolution with a dynamic range of 4096 gray levels; for the analog fracture considered in these experiments, pixel size was on the order of 2 x10^{-4} cm^2. Optical contrast was enhanced by staining the experimental fluid; a mixture of 1g FD&C blue #1 to 1 liter of de-ionized water was used. Wetting properties of the experimental fluid were evaluated using glass capillary tubes, and found to be consistent with de-ionized water.

aperture structure characterization

Mean aperture and saturated conductivity of the analog fracture were measured directly, while spatial variation in the aperture field was characterized using simple light absorption theory. The mean aperture (â = 0.0215 cm) was measured by volumetric imbibition into the fracture under dry initial conditions. Measured saturated conductivity was 2.89 cm/s at a Reynolds Number (R_e) of 3.1; in previous experiments[7] using this analog fracture, K_s was found to remain constant for R_e between 0.27 and 5.93.

Each pixel of the imaging array records the luminous intensity (I) of light transmitted through a small region of the analog fracture. The absorption of light (initial intensity = I_o) by a series of substances of thickness (d_i) with absorption coefficients (α_i) is given by Lambert's Law (equation 2).

$$I = I_o \exp^{-(\alpha_1 d_1 + \alpha_2 d_2 + \ldots)} \qquad (2)$$

In order to measure the aperture, d_{ap}, it is necessary to decouple light absorption due to fluid within the aperture from that caused by the rest of the test cell and fracture plates. This is done by collecting an intensity image from the fracture saturated with a clear fluid (I_{cl}) and saturated with a dyed fluid of equivalent refractive index (I_d). In order to minimize dispersion caused by the textured glass surface, a base solution of 135% by weight sucrose was used to match refractive indices with the glass; the dyed solution also contained 0.25 gm per liter of FD&C blue #1 dye. Recorded light intensity of the dye filled fracture is given by:

$$I_d = I_{cl} \exp^{-\alpha_d d_{ap}} \qquad (3)$$

Equation 3 is first solved for $a_d d_{ap}$ at each pixel location within the aperture field. This result is then normalized using the measured mean of all $a_d d_{ap}$ values. Multiplication of the normalized aperture field by the measured mean aperture (â) of the analog fracture yields the spatial structure of the aperture field at the pixel scale; the resulting aperture distribution is shown as Figure 1. Subdividing the aperture domain into pixels implicitly averages the local data; therefore, the

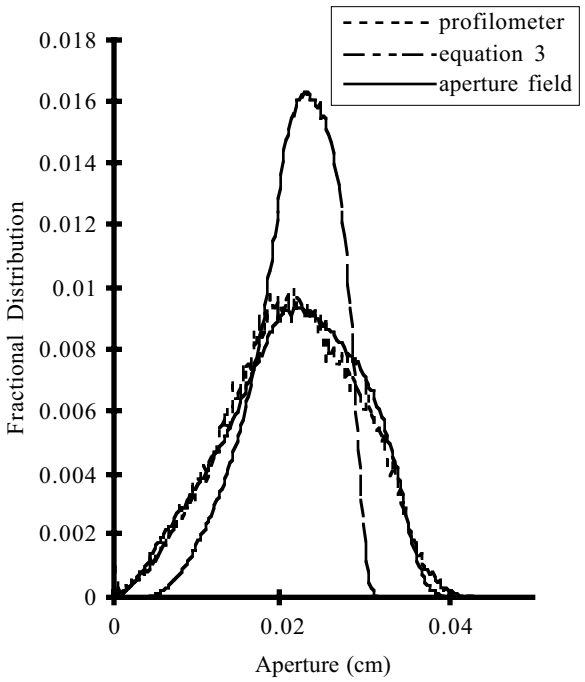

Figure 1: Aperture Distribution of Analog Fracture: Aperture distribution of the analog aperture field is shown, along with distributions of the aperture field as predicted by Lambert's Law and a numerical model based on profilometer measurements as presented by Glass[8].

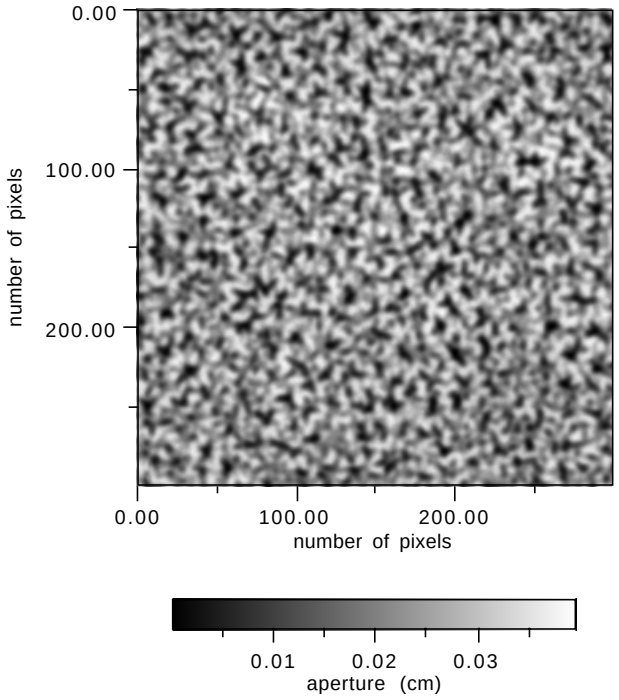

Figure 2: Spatial Structure of Model Aperture Field: A 5 cm square section of the model aperture field is shown in gray scale. Axes indicate size of the section in pixels, while the color bar indicates aperture size.

distribution of d_{ap} given by equation 3 does not wholly capture the full range of apertures known to occur within the analog fracture. The range should extend from 0 at contact points to approximately twice the mean aperture, rather than the range of 0.004 to 0.032 cm as obtained from equation 3. In order to correct for these discrepancies, the aperture field was adjusted through multiplication by a stretch factor that varied linearly with aperture between its lowest value (d = 0.004 cm) and its highest value (d = 0.032 cm), such that the expected minimum and maximum values were preserved (Figure 1). Aperture distribution of a numerical model of this analog fracture based on profilometer measurements is shown for comparison[8]. A gray-scale image, depicting spatial structure of the reconstructed aperture field is presented as Figure 2; for clarity, only a small section (~5 cm square) is shown.

phase structure delineation

In order to evaluate phase saturation and structure, it is necessary to delineate the spatial distribution of each phase. Pixels were assumed to be occupied fully by a single phase; as pixel size is slightly smaller than the mean aperture, this is a reasonable assumption. Differences in light attenuation between the phases were used to transform phase structure images into binary arrays. In these arrays, pixels occupied by the wetting and non-wetting phases are represented by 0's and 1's, respectively. Light passing through a single phase of variable thickness produces a distribution of intensities.

Assuming that light scattering at phase interfaces has a minimal effect, the distribution of intensities collected from a two-phase structure will be the sum of the individual distributions. Where the light absorbencies of the two phases are significantly different, the composite distribution will show two distinct local maxima, such as that seen in Figure 3; the dashed lines illustrate postulated distributions associated with individual phases. It is assumed that the central minimum of the composite distribution (I_c in Figure 3) provides a minimum error estimate for delineating phase occupation on the basis of pixel intensity. For the two-phase system considered here (air and water), pixels with intensity values below I_c are assumed to be occupied by the wetting phase while those above I_c are assumed to be filled with the non-wetting phase.

Preliminary investigations demonstrated that a single value of I_c was not appropriate for the relatively large domain considered here (1.65×10^6 pixels). This problem was resolved by operating on sub-regions of the image, 128 x 128 pixels in size, such as that shown in Figure 4a. While comprising less than 1% of the total image, each region contains sufficient information to form an appropriate histogram (16384 pixels) as shown in Figure 4b. Prior to determining the central minimum, an inverse distance weighted moving average algorithm was used to smooth the histogram, eliminating spurious local features. The smoothed histogram was then searched to find the two most significant

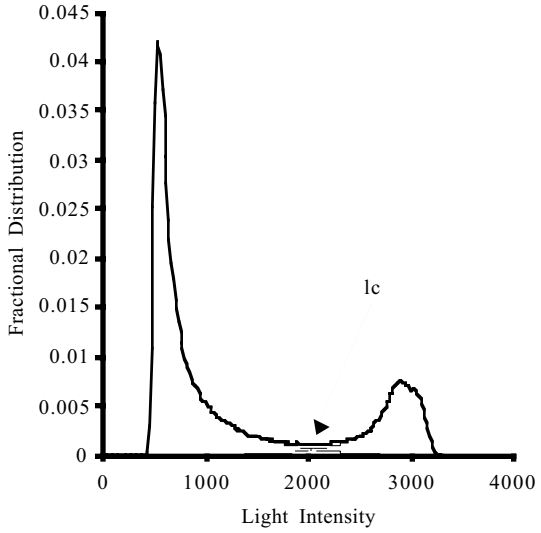

Figure 3: Distribution of Light Intensity in an Image of a Two-Phase Structure: This histogram shows the distribution of intensities collected from experiment 3-3 (shown as Figure 5c). The low intensity mode of this composite histogram is associated with pixels filled by the wetting phase and the high intensity mode with the non-wetting phase. While the exact shape of the individual distributions is unknown, the dashed lines are used to illustrate likely forms for the individual distributions.

local maxima and the associated central minimum, which was taken to represent I_c for that sub-region. All pixels within the sub-region that are less than I_c are set to 0 and the remainder are set to 1 (Figure 4c). This procedure was then repeated for all such sub-regions within the image. Multiplication of this binary array by the reconstructed aperture field yields the three-dimensional spatial structure of the non-wetting phase. By reversing 0's and 1's within the binary array, spatial structure of the wetting phase is obtained.

Results and Discussion

Seven experiments were performed, each with a different phase structure. As discussed below, three different methods were used to form the phase structures. Steady-state flow of the non-wetting phase was established prior to measurement of K. Images collected before and after permeability measurements were used to verify stability of the wetted structure. These images were also used to measure wetting phase saturation and spatial distribution of the phases; experimental data is summarized in Table 1. After each measurement, a series of computer controlled solenoid valves were used to introduce a sharp tracer front across the full width of the analog fracture. Subsequent images of tracer advancement serve to illustrate channeling of flow by the phase structure; thereby providing qualitative information regarding the effects of phase structure on flow path length and spatial variation in the cross-sectional area available for flow.

Exp #	S_w	k_r	$\hat{a}_w$	$\frac{\hat{a}_w}{\hat{a}}$	τ	Type
1-1	.906	0.715	.0209	.975	.831	1
1-2	.955	0.887	.0212	.989	.949	1
2-1	.554	0.109	.0183	.852	.272	2
2-2	.617	0.148	.0189	.881	.310	2
3-1	.676	0.197	.0194	.907	.355	3
3-2	.640	0.145	.0191	.891	.285	3
3-3	.663	0.160	.0194	.902	.297	3

Table 1

formation of phase saturations and structures

Three general classes of structure were considered; the first (Type 1) was intended to be consistent with assumptions of thermodynamic equilibrium between phases, while the others (Type 2 & 3) reflect non-equilibrium phase invasion processes. Current conceptual models of fracture/matrix interaction assume that at equilibrium, matric pressure introduces an aperture cutoff defined by capillary bundle theory (e.g. Wang and Narasimhan[6]); all apertures smaller than this cutoff will be filled with the wetting phase, while the non-wetting phase will occupy all apertures larger than the cutoff. Since phase structures reach equilibrium through matrix flow, film flow, and evaporative redistribution, the physical and temporal constraints imposed by our experimental system prohibited creation of true equilibrium phase structures. However, it was hypothesized that alternative means could be used to distribute the non-wetting phase such that it occupies only the largest apertures, thereby capturing the salient feature of equilibrium theory. Type 1 phase structures were created starting with a two-phase structure containing a significant air fraction. A transient wetting phase flow was then induced thorough intermittent application of fluid pressure. This procedure acted to drive the non-wetting phase out of the small apertures and allowed it to lodge in the large apertures. The resultant wetted structure consisted of small, compact inclusions of the non-wetting phase which, like the large apertures, were distributed throughout the fracture (see Figure 5a). Physical constraints on redistributing the air fraction limited exploration of such structures to large wetting phase saturation (S_w = 0.9-0.95).

Non-equilibrium processes are expected to affect wetted structure genesis, fluid entrapment, and thus k_r. Glass and Norton[9] have shown that in-plane trapping mechanisms act to prevent aperture filling from the matrix according to capillary bundle theory. In order to explore the effects of phase structure established by non-equilibrium processes on k_r, more complicated Types 2 and 3 phase saturation structures were created. Type 2 structures were formed by first draining a saturated fracture and then establishing liquid flow. Drainage of a saturated fracture through application of suction leaves the residual wetting phase distributed about the fracture as disconnected blobs. Subsequent application of steady wetting phase flow across the full fracture width creates a

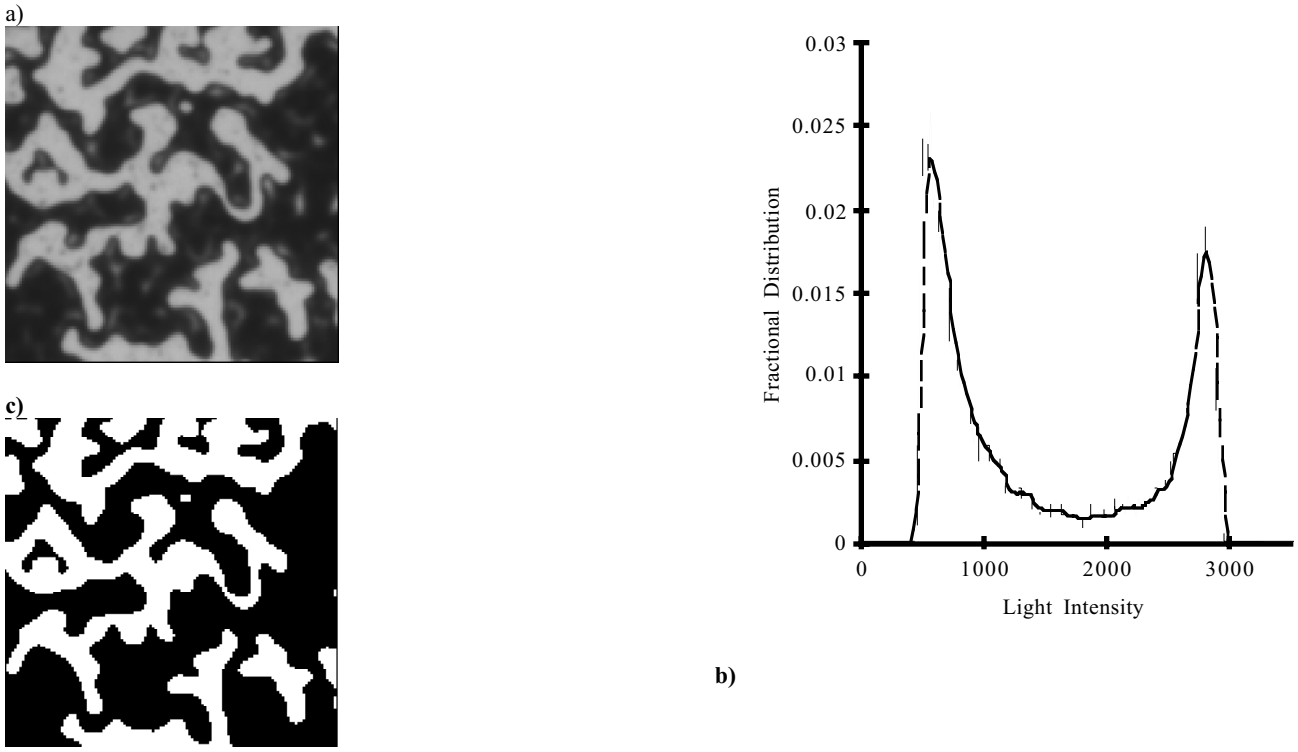

Figure 4: Delineation of Phase Structure: a) Sub-region of experiment 3-3 measuring 128 x 128 pixels, dark regions are filled with the wetting phase and light regions with the non-wetting phase; b) Histogram of Figure 4a, solid line shows results of smoothing algorithm. Note that the minimum of this sub-region is better defined than that for the entire image (Figure 3); c) Binary transformation of Figure 4a showing the wetting phase as black and the non-wetting phase as white.

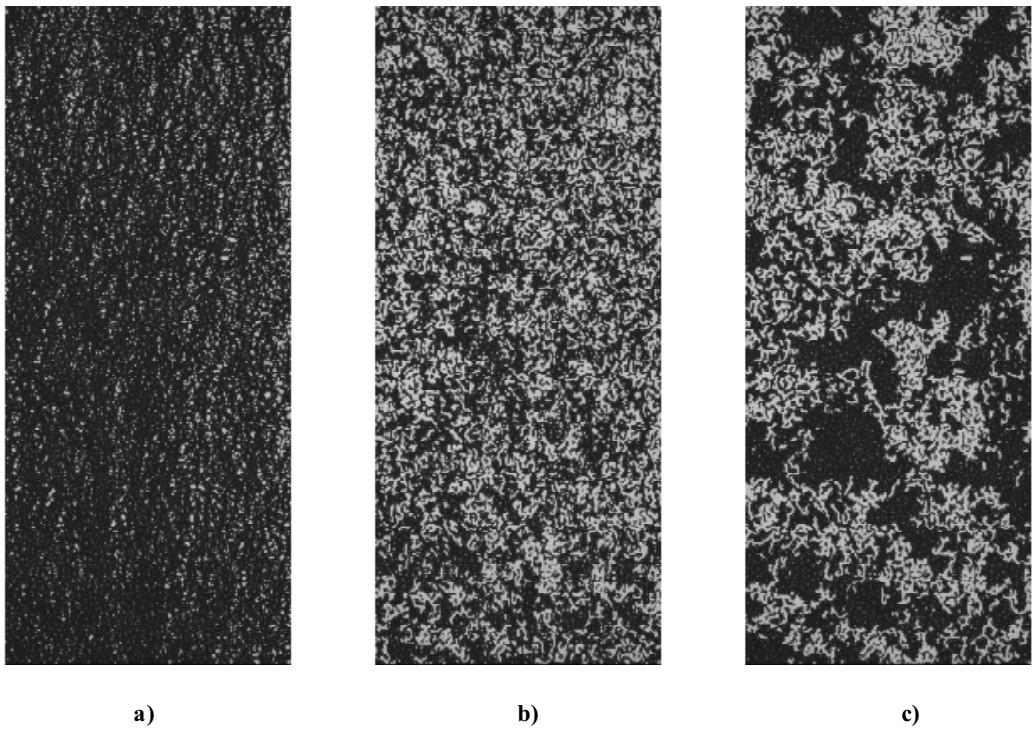

Figure 5: Types of Wetted Structure Considered: a) Type 1 (exp. 1-1); b) Type 2 (exp. 2-1); c) Type 3 (exp. 3-3).

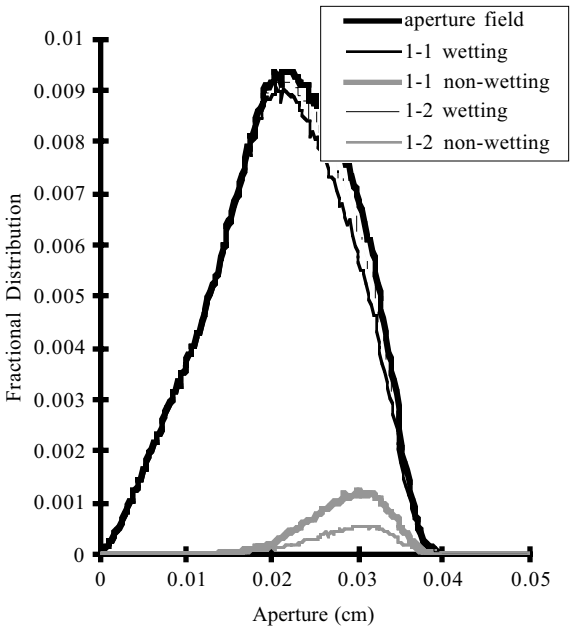

a)

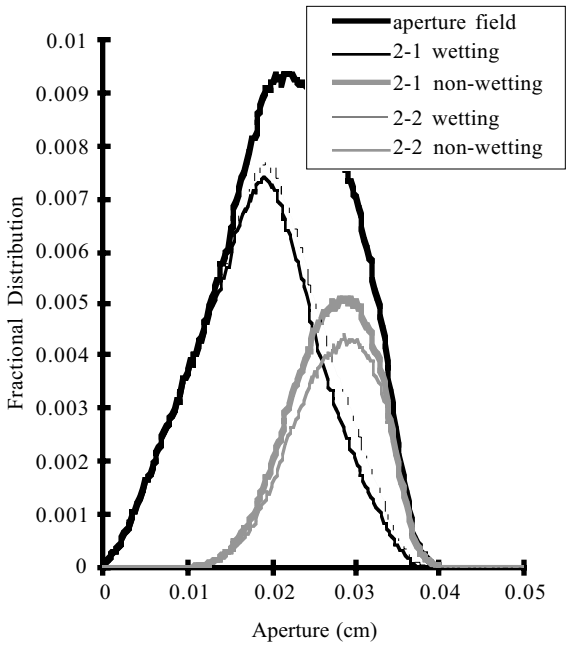

b)

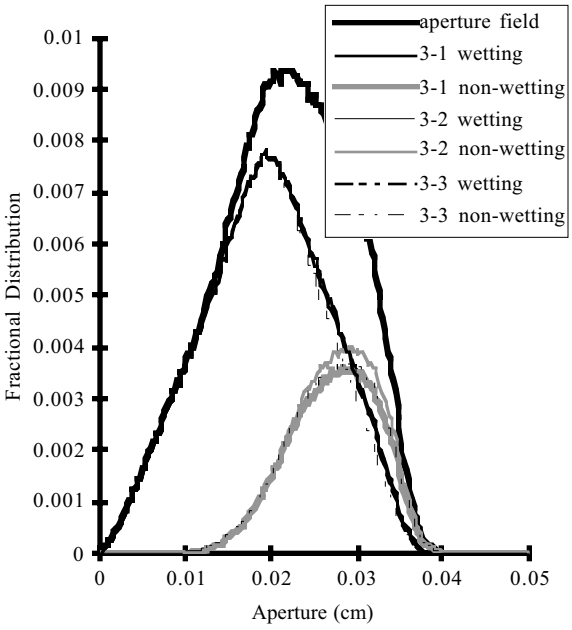

c)

Figure 6: Distribution of Air in Entrapped Regions: Normalized distribution of air filled apertures in each type of structure is shown. Distribution of the model aperture field is shown for comparison. a) Type 1; b) Type 2; c) Type 3.

structure containing pervasive entrapped non-wetting phase regions (Figure 5b). Type 3 structures were formed by slow gas injection from one end of a saturated fracture followed by establishing liquid flow. Slow gas injection along the plane of a saturated fracture under quasi-static conditions creates a very complex, fully connected non-wetting phase. Subsequent application of steady wetting phase flow across the full fracture yields increased connectivity within the non-wetting phase as compared to the Type 2 structures (Figure 5c). Saturations for both Type 2 and 3 structures were significantly lower than for the Type 1 structures. No attempts were made to systematically vary saturation; phase structures were formed and then saturation measured.

analysis of phase aperture residence and saturation structure

Normalized distributions of apertures filled with the wetting and non-wetting phases for Type 1, 2, and 3 structures are shown in Figures 6a, 6b, and 6c respectively; the aperture field distribution is shown for comparison. As expected, for all structural types, the non-wetting phase preferentially occupies the largest apertures. However, in contrast to equilibrium theory, in all phase structures considered, there is significant overlap between the phase distributions. In the Type 1 structures, which were intended to mimic equilibrium theory, the non-wetting phase did not occupy all of the largest apertures and filled a relatively broad range of aperture sizes. Thus, our procedure for creating Type 1 phase structures did not fully simulate aperture filling according to capillary bundle theory. Since transient pressures were applied to break up and mobilize entrapped non-wetting phase regions, pressures may not have been of sufficient magnitude to dislodge the non-wetting phase from moderately large apertures or fully break-up the non-wetting phase. In the Type 2 and 3 phase structures, which were formed under non-equilibrium conditions, the non-wetting phase occupies a

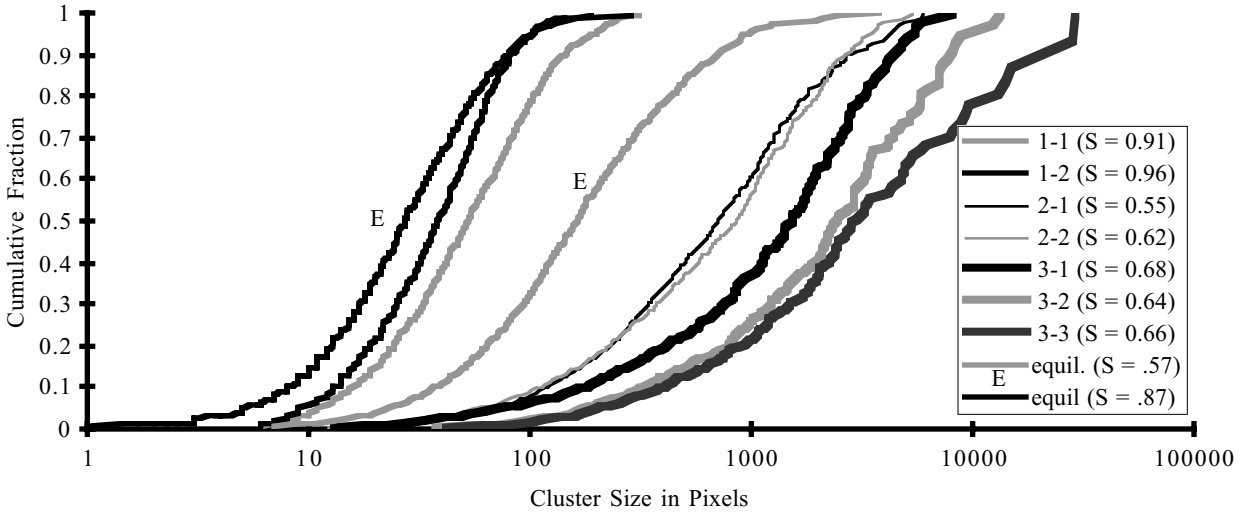

Figure 7: Distribution of Entrapped Phase: Connected regions occupied by the non-wetting phase are identified as individual clusters. Normalized cumulative distributions of cluster sizes are shown for each experimental phase structure. For comparison, cluster size distributions for phase structures predicted by capillary bundle theory (S_w = 0.65, 0.89) are also shown.

broader range of aperture scales than observed for the Type 1 structures.

Connected apertures filled with the non-wetting phase are identified as individual clusters, which then can be characterized with respect to size, shape, and spatial location. The non-wetting phase cluster size distribution for each of the experiments is shown in Figure 7. Type 1 structures show a span of nearly 2 orders of magnitude while Types 2 & 3 span nearly 3 orders. In addition, size of the largest cluster increases as we pass from type 1 to 2, and on to 3. It is instructive to compare the cluster size distributions formed in our experiment to those that would be formed on our aperture network assuming equilibrium theory. A series of equilibrium phase structures were modeled by defining all apertures on the network smaller than an arbitrarily selected cutoff as filled with the wetting fluid. Non-wetting phase cluster size distributions for two different equilibrium structures (S = 0.57, S = 0.87) are also shown on Figure 7. When compared to equilibrium structures at similar saturations, our experiments tend to larger clusters, and a larger range of cluster sizes. Structures formed under non-equilibrium processes (Types 2 & 3) show order of magnitude differences in the cluster size distribution when compared to an equilibrium structure formed at a similar saturation. Cluster size distributions for Type 1 structures are similar in shape to the equilibrium model, however both examples plot to the right of an equilibrium structure at lower saturation, indicating that entrapped clusters are generally larger in the Type 1 structures than predicted by capillary bundle theory. Even though aperture filling in Type 1 structures was not strictly in accordance with equilibrium theory and non-wetting phase clusters were larger than expected, both spatial distribution of the clusters and phase connectivity appeared to be very similar to that predicted by the equilibrium model. Therefore, we assume that for the purposes of this study, Type 1 structures provided a reasonable approximation of equilibrium conditions at high liquid saturation.

relative permeability

Before considering relative permeability, we first discuss saturated permeability of the analog fracture. The simplest model for single phase flow through a fracture of aperture a and cross-sectional area A (A = a • fracture width) is to use Darcy's Law, with hydraulic conductivity approximated by the parallel plate law (e.g., Bird et al.[10]):

$$Q = -AK\nabla\phi \tag{4a}$$

$$K = \frac{\rho g a^2}{12\mu} \tag{4b}$$

where Q, $\rho, \mu, g,$ *and* ϕ represent volumetric flow, fluid density, fluid viscosity, gravitational constant, and pressure-head, respectively. Hydraulic conductivity of the analog fracture used in these experiments was measured at 2.89 cm/s; equation 4b gives the equivalent hydraulic aperture as 0.0178 cm, which is approximately 17% smaller than the measured mean aperture (0.0215 cm). The observed discrepancy occurs because the parallel plate model does not fully describe the physics of flow through a variable aperture field[11]. Primary mechanisms unaccounted for in the parallel plate model are deviation from a linear path and converge/divergence of flow normal to the fracture plane. Flow through a rough walled fracture does not follow a perfectly linear trace along the fracture plane as assumed in the parallel plate model. If all other hydraulic parameters are held constant, resistance to flow will increase linearly with length of the flow path. In the

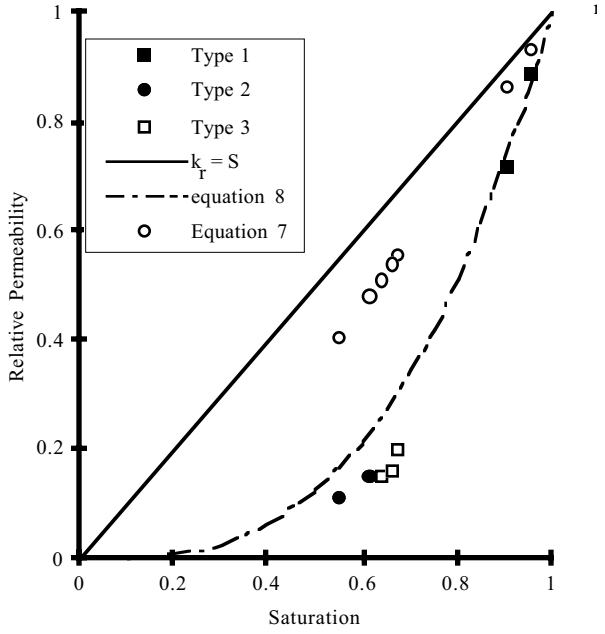

Figure 8: Relative Permeability as a Function of Wetting Phase Saturation

analog fracture considered here, tracers were used to visualize in-plane variation in the flow path. Under saturated conditions, macroscopic deviation from a linear path was observed to be relatively small. However, small wavelength variations may add significantly to the path length; thereby accounting for a large portion of the observed deviation from equation 4b. It is expected that flow resistance resulting from the convergence and divergence of flow paths normal to the fracture plane as flow passes through the variable aperture field is responsible for most of the remaining discrepancy. Mean aperture does not contain sufficient information to fully characterize flow within a variable aperture field, but can be regarded as a reasonable first order approximation.

In the preceding paragraph, factors contributing to the saturated hydraulic conductivity of a variable aperture fracture were considered. We now assemble a model of wetting phase relative permeability in a horizontal fracture under steady state conditions. In the experiments presented here, the non-wetting phase was immobile, and except at the phase interface, the non-wetting phase fully spans the aperture gap. As a result, apertures occupied by the non-wetting phase act as impermeable barriers within the aperture field, analogous to areas within the fracture that are in direct contact. In order to explain the observed rapid decrease in k_r with S_w (Figure 8, Table 1), we first consider processes acting on the distributed or average properties of the two-phase structure.

Lowering wetting phase saturation reduces the cross-sectional area available for wetting phase flow. Darcy's Law defines permeability as a proportionality constant relating volumetric flow to pressure gradient and cross-sectional flow area. Changing phase saturation does not alter the cross-sectional area of the fracture, but actually controls the portion of that area that is available for flow. As this modifier acts on the flowing phase, not the fracture, it is typically included in k_r. From the geometric properties of the system, it is logical to expect that a first order approximation for k_r would take the following form:

$$k_r = S_w \tag{5}$$

Fractured-reservoir simulators used by the petroleum industry typically make this assumption[12] which is shown as the solid line in Figure 8. While this simple model does not fit the data well, it does account for a significant portion of the observed decrease in k_r with S_w. For the homogenous, isotropic analog fracture considered here, continuity implies that S_w will provide an upper bound on k_r. As it is possible to conceptualize aperture structures where S_w will not provide an upper bound on k_r, this observation should be generalized with caution.

A second process acting on k_r is the preferential occupation of smaller apertures by the wetting phase. Under two phase conditions, the mean aperture occupied by the wetting phase ($\hat{a}_w$) is expected to be smaller than the mean aperture of the fracture ($\hat{a}$). As hydraulic conductivity is assumed to be proportional to the aperture squared (equation 4b), this observed redistribution will have a different effect on k_r than the simple reduction in cross-sectional area discussed above. Substitution of mean aperture into equation 4b provides a first-order estimate of K_s for a rough-walled fracture; therefore, mean aperture occupied by the wetting phase is expected to display a similar relationship for permeability under two-phase conditions. Assuming that all quantities in equation 4b except mean aperture are constant, solution of equation 1 for k_r yields:

$$k_r \propto \frac{\hat{a}_w^2}{\hat{a}^2} \tag{6}$$

As discussed above, convergence and divergence of the aperture field contributes to a discrepancy between mean and hydraulic apertures of the analog fracture. If the distributions of a and a_w are similar, taking the ratio of the means, as done in equation 6 is expected to cancel out much of this discrepancy. Equations 5 and 6 may then be combined to produce an improved model for relative permeability based solely on average properties of the phase structure (equation 7).

$$k_r \propto \frac{\hat{a}_w^2}{\hat{a}^2} S_w \tag{7}$$

If apertures within the fracture are filled in accordance with capillary bundle theory, the ratio of $\hat{a}_w$ to $\hat{a}$ will equal S_w, collapsing equation 7 to:

$$k_r \propto S_w^3 = \frac{\hat{a}_w^3}{\hat{a}^3} \tag{8}$$

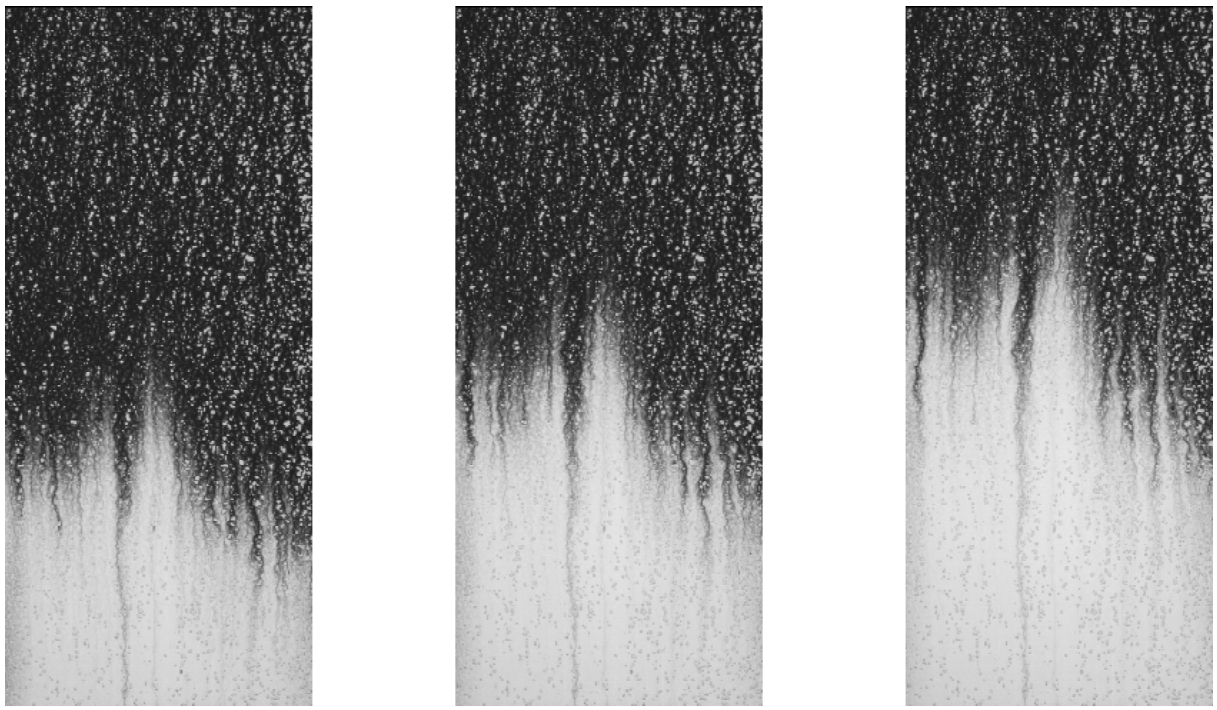

a) **b)** **c)**

Figure 9: Flow Path Visualization: Movement of a tracer pulse released from the left side of the fracture into the wetted structure shown as Figure 5a (experiment 1-1).

We note that equation 8 is identical to one presented by Wang and Narasimhan[6] except for their inclusion of a tortuosity factor (τ).

The model given by equation 8 is observed to fit the data reasonably well (Figure 8), particularly at large saturations. However, in the experiments presented here, aperture filling was not strictly in accordance with capillary bundle theory; hence S_w is not a good approximation for the ratio of $\hat{a}_w$ to $\hat{a}$, as assumed in equation 8. Predictions based on equation 7 do not fit the data nearly as well as equation 8 (Figure 8). This does not imply that equation 8 is a more appropriate model, merely that factors unaccounted for in either equation 7 or 8 are significant and must be included.

As models based on distributed properties of the phase structure (equation 7) are unable to fully account for observed behavior, we must consider the effects of phase structure. To explore channelization of flow induced by phase structure, at the conclusion of each experiment a tracer consisting of pure de-ionized water was released as a sharp pulse across the full width of the analog fracture. Figures 9, 10, and 11 illustrate tracer advancement through the phase structures seen in Figure 5a, b, and c, respectively. Even the relatively simple Type 1 phase structures act to channelize flow (Figure 9), breaking up the front into individual channels and retarding advancement in areas of relatively large non-wetting phase saturation (along the bottom edge). In the more complex Type 2 structure (Figure 10), channelization becomes more distinct but the front still advances more or less uniformly across the full fracture width. In Type 3 structures (Figure 11), flow appears constrained to two or three primary channels that follow tortuous paths through this complicated phase structure.

It is apparent from Figures 9-11 that phase structure acts to channelize flow, and that the degree of flow modification is related to complexity and connectivity of the non-wetting phase structure. Two processes that act to decrease permeability are path length and localized variation in channel width. At the low saturations exhibited by Type 2 and 3 structures, path length will be significantly longer than expected under fully saturated conditions. As permeability is expected to demonstrate a linear relationship with path length, this process is believed to account for much of the discrepancy between equation 7 and measured data. The increased complexity of the Type 3 structures creates longer wavelengths in the flow path than in the Type 2 structures. However, average path length is not necessarily any longer in the Type 3 structures.

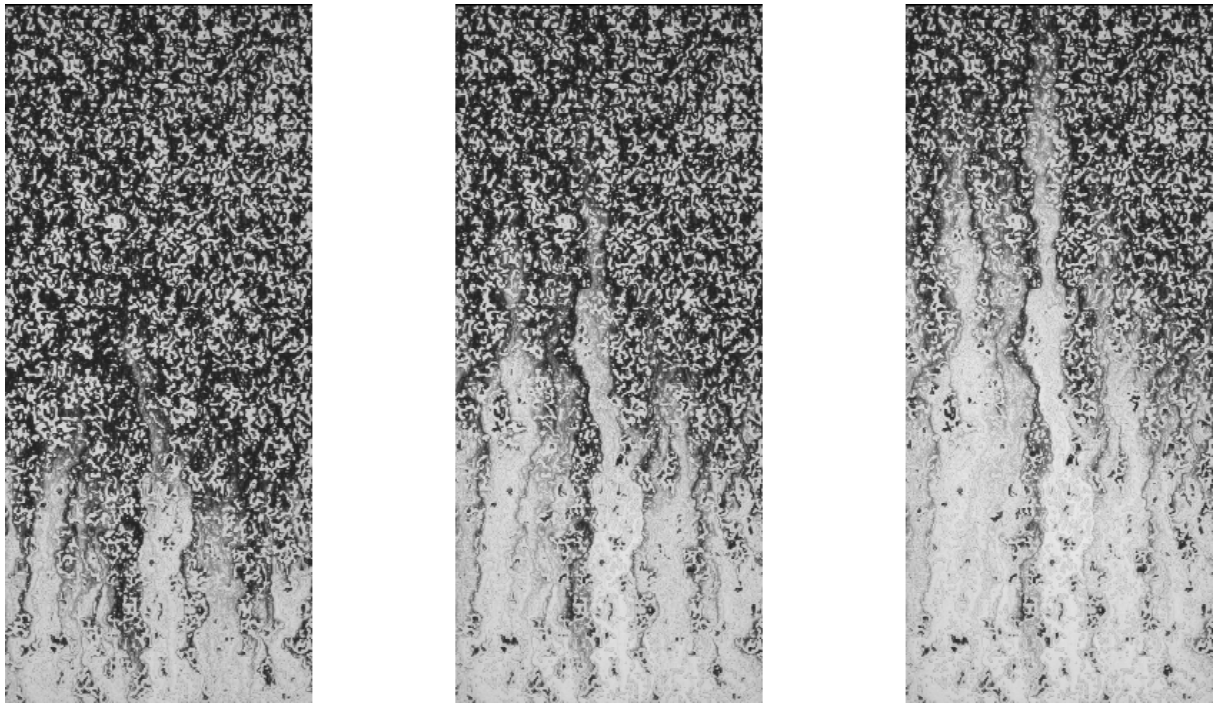

a) **b)** **c)**

Figure 10: Flow Path Visualization: Movement of a tracer pulse released from the left side of the fracture into the wetted structure shown as Figure 5b (experiment 2-1).

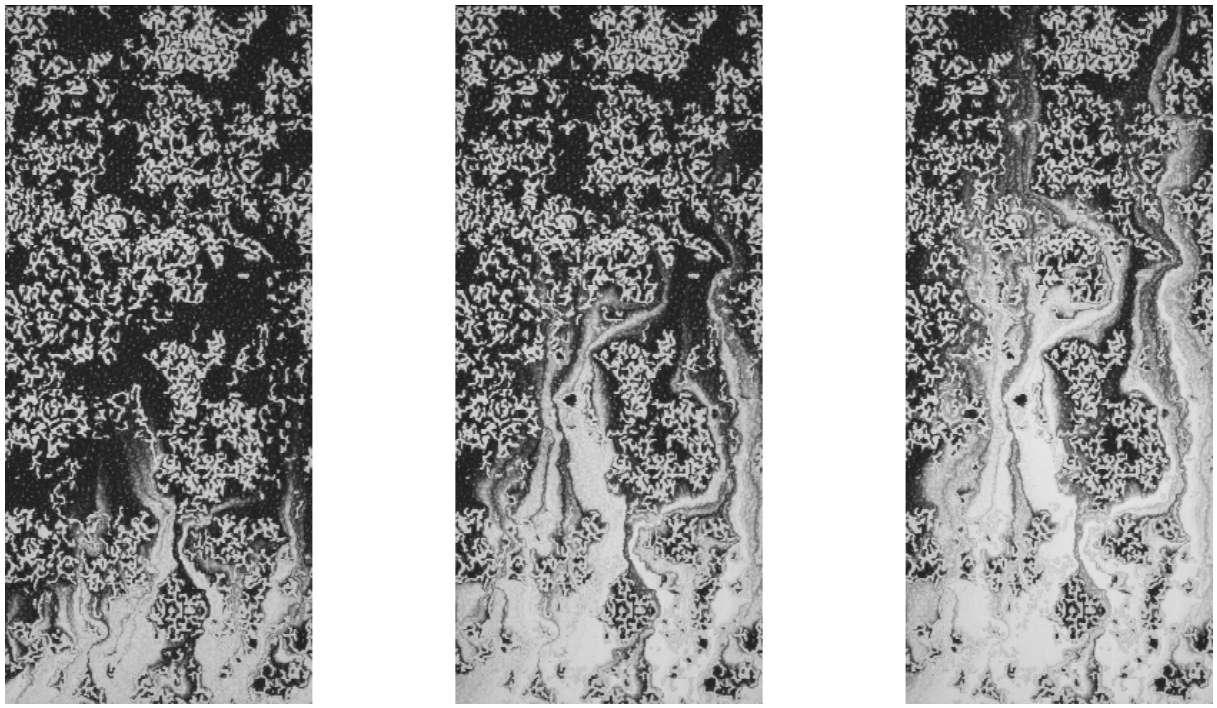

a) **b)** **c)**

Figure 11: Flow Path Visualization: Movement of a tracer pulse released from the left side of the fracture into the wetted structure shown as Figure 5c (experiment 3-3).

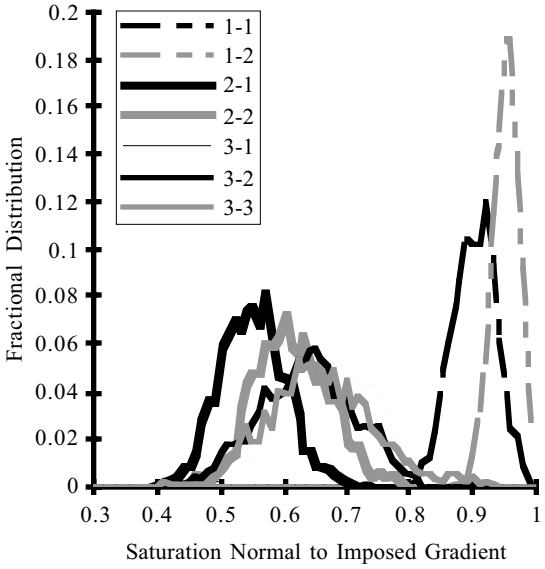

Figure 12: Saturation Normal to Imposed Gradient: Saturation normal to the imposed gradient provides a first order approximation of local cross-sectional area open to flow. Fractional distributions show that Type 3 structures exhibit the most variation and are hence most likely to contain choke points.

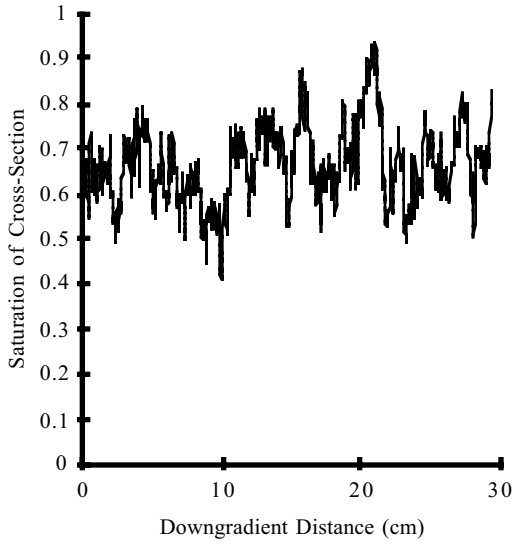

Figure 13: Variation in Cross-Sectional Flow Area: Saturation integrated along a cross-section normal to the imposed gradient is shown for experiment 3-3.

The channels created by the two-phase structure are not of uniform width. Therefore, relatively large amounts of fluid are forced to pass through narrow "choke points" that act to restrict flow, causing large localized pressure drops. Pyrak-Nolte et. al.[13] concluded that fracture permeability is controlled by the largest connected channel within the system and that flow through that channel is controlled by its' narrowest aperture, or choke point. Measurement of saturation along a linear trace perpendicular to the imposed gradient provides a first order approximation of cross-sectional flow area; distributions of all such traces are presented as Figure 12. It is apparent that variation in cross-sectional flow area increases with structural complexity and connection of the entrapped phase. Therefore, Type 3 structures will be the most likely to experience flow constriction at choke points. This observation is affirmed by qualitative evaluation of tracer pulses (Figures 9-11) and illustrated by displaying variation in cross-sectional area along the Type 3 structure of experiment 3-3 (Figure 13, see also Figure 5c). This analysis does not imply that Type 3 structures have the narrowest channels, simply that flow along those channels are likely to experience the most variation in area and hence local pressure drop. The significance of choke points will decrease with increasing number of flow channels and interconnection between the channels.

Further analysis of phase structure must be accomplished in combination with numerical simulation before the relative importance of choke points and channelization can be determined and quantified; for now we take the conventional approach and bundle the effects of phase structure into a single parameter, tortuosity (τ).

$$k_r = S_w \tau \frac{\hat{a}_w^2}{\hat{a}^2} \qquad (9)$$

This relationship is a modification of one presented by Wang and Narasimhan[6] with differences in the assumptions regarding aperture filling, as stated previously. Equation 9 was used to calculate τ for the experiments presented here; values are given in Table 1. As expected, phase structure has a much smaller effect on k_r in Type 1 structures than in either Type 2 or Type 3 structures. This is most likely due to the large difference in S_w between the structural types, rather than any effects induced by the specific structural forms. Even though Type 2 and 3 structures appear to be very different, there was no distinguishable difference in measured τ between the two. Therefore, it may be possible to write τ as a function of S_w for some broader class of structures that would encompass Types 1, 2 and 3. Development of such a relationship will require an in depth exploration into structural control of path length and choke points, as well as the effects of these processes on k_r.

While the experiments presented here imply that τ is a strong function of saturation and a weak function of phase structure, that conclusion may not be universally true. Non-equilibrium processes, such as the gravity-driven wetting front instability demonstrated by Nicholl et al.[7], may act to reduce τ by creating oriented wetted structures. In inclined fractures, the effects of gravity can destabilize a wetting front, leading to

the development of fingers oriented in the direction of gravity. At times short with respect to matrix imbibition and evaporative redistribution, moisture left by the passage of individual fingers is expected to create preferential pathways for subsequent flow[14]. These pathways may then lead to development of a wetted structure oriented in the direction of gravity, analogous to a series of parallel channels. In such a scenario, spatial structure of the wetted phase is expected to exhibit significant, and perhaps dominant control over τ. Wetted structures formed by other non-equilibrium processes may also significantly effect τ, and hence k_r.

Finally, we note that while results presented here imply that k_r is a weak function of phase structure, spatial structure of the phases will almost certainly have a significant effect on transport properties. Type 3 structures such as that shown in Figure 11, act to channelize flow into discrete channels, which in turn are expected to act as rapid pathways. Furthermore, complexity of the structure creates large "dead" zones analogous to dead-end pores in porous media. As a result, the residence time distribution for tracer movement through a Type 3 structure is expected to differ significantly from that associated with a Type 2 structure of similar permeability. Similar situations are seen to occur when considering saturated flow through heterogeneous porous media; structure is observed to exhibit minimal control on effective permeability while exhibiting significant control on transport properties (e.g. Smith and Schwartz[15]; Yeh[16]).

Conclusions

We have used simple light absorption theory to develop a methodology for characterization of aperture and phase structure within a transparent analog fracture. In addition to providing detailed spatial characterization of the aperture field, this technique provides a means of measuring phase complexity in the fracture plane and exploring the distribution of apertures occupied by both wetting and non-wetting phases. The techniques developed were used to explore wetting phase relative permeability under steady-state flow conditions in the horizontally oriented analog fracture.

As expected, in all phase structures considered, large apertures were preferentially occupied by the non-wetting phase. In phase structures formed by mimicking potential non-equilibrium field processes, the non-wetting phase occupied a significantly wider distribution of apertures than predicted by equilibrium theory. Detailed measurements were used to explore a simple process oriented model for relative permeability. Parameters incorporated in the model include wetting phase saturation (S_w), mean aperture occupied by the wetting phase ($\hat{a}_w$), and a structural complexity term. Phase saturation was shown to be an inadequate estimator of $\hat{a}_w$, except for large wetting phase saturation ($S_w > 0.9$) structures similar to those expected to form under the equilibrium assumptions of capillary bundle theory. Distributed parameters (S_w and $\hat{a}_w$) were shown to be insufficient to model relative permeability in the low wetting phase saturation (S_w = 0.55-0.66) structures considered. Tortuosity and localized flow restriction were observed to reduce relative permeability by as much as 70% in such phase structures. Effects of spatial structure on k_r were not observed to vary greatly between phase structures of similar saturation but differing complexity; however phase structure is expected to have a marked effect on transport properties of the system.

Field scale numerical models for use in performance assessment in unsaturated fractured rock at Yucca Mountain cannot explicitly model individual fractures in detail; therefore, effective property models which properly include two-phase flow in fractures must be developed. The investigation presented here describes the first steps towards development of process oriented models of fracture hydraulic properties under two-phase flow conditions. Subsequent development and testing involves both physical and numerical experimentation. Cast replicas of natural tuff fractures from Yucca Mountain will be used in experimentation similar to that accomplished here in a simple analog rough-walled fracture. Since we will never be able to understand the behavior of all fractures at Yucca Mountain from a small set of cast natural replicas, we are also developing the technology to directly manufacture analog fractures through numerically controlled milling techniques. This will allow systematic exploration into the hydraulic effects of various aperture properties, including mean aperture, correlation length, roughness length scales, aperture heterogeneity, and anisotropy. Milled fractures will be replicated using transparent casting compounds to allow flow visualization; by varying the casting technique, surface wetting properties can also be varied. To limit the number of manufactured fractures required, aperture scale numerical models, once properly tested, will be used to obtain additional data. This experimental and numerical investigation will identify the essential fracture characteristics required for modeling hydraulic behavior under two-phase flow conditions. Such characteristics and valid simplifications of models for two-phase fracture flow will then be incorporated into a properly formulated effective property model for inclusion in the performance assessment exercises at Yucca Mountain.

ACKNOWLEDGMENTS

The authors gratefully acknowledge the assistance and support provided by the following: W.C. Ginn in design and fabrication of the experimental apparatus; L. Orear in development of image acquisition software; P.B. Davies, C.H. Ho, and S.W. Webb for their careful and constructive reviews. This work was supported by the U.S. Department of Energy, Office of Civilian Radioactive Waste Management, Yucca Mountain Site Characterization Project Office, under contract DE-AC04-94AL85000.

Nomenclature

a	-	fracture aperture
$\hat{a}$	-	mean aperture
a_w	-	aperture occupied by wetting fluid
$\hat{a}_w$	-	mean aperture occupied by wetting fluid
A	-	cross-sectional flow area
d	-	thickness of absorptive material
d_{ap}	-	thickness of aperture
g	-	gravitational constant
I	-	luminous intensity
I_c	-	intensity used to delineate between phases
I_{cl}	-	intensity associated with clear fluid
I_d	-	intensity associated with dyed fluid
I_o	-	initial intensity
k_r	-	relative permeability
K	-	hydraulic conductivity
K_s	-	saturated hydraulic conductivity
Q	-	volumetric flow rate
R_e	-	Reynolds number
S_w	-	wetting fluid saturation
α	-	light absorption coefficient
α_d	-	absorption coefficient for dye
μ	-	fluid viscosity
ρ	-	fluid density
ϕ	-	pressure head
τ	-	tortuosity

REFERENCES

1. R.W. Barnard, M.L. Wilson, H.A. Dockery, J.H. Gauthier, P.G. Kaplan, R.R. Eaton, F.W. Bingham, and T.H. Robey , "TSPA 1991: An Initial Total-System Performance Assessment for Yucca Mountain", SAND91-2795, Sandia National Laboratories, Albuquerque, NM, (1992).

2. J.R. Murphy, and N.R Thompson, "Two-Phase Flow in a Variable Aperture Fracture", Water Resources Res., 29, 10, 3453-3476, October, (1993).

3. P.W. Reimus, B.A. Robinson, and R.J. Glass, "Aperture Characteristics, Saturated Fluid-Flow, and Tracer Transport Calculations for a Natural Fracture", Proceedings of the Fourth Annual International Conference on High Level Radioactive Waste Management, Las Vegas, Nevada, April 26-30, (1993).

4. B.L. Cox, and J.S.Y. Wang, "Single Fracture Aperture Patterns: Characterization by Slit-Island Fractal Analysis", Proceedings of the Fourth Annual International Conference on High Level Radioactive Waste Management, Las Vegas, Nevada, April 26-30, (1993).

5. P. Persoff, and K. Pruess, "Flow Visualization and Relative Permeability Measurements in Rough-Walled Fractures", Proceedings of the Fourth Annual International Conference on High Level Radioactive Waste Management, Las Vegas, Nevada, April 26-30, (1993).

6. J.S.Y. Wang, and T.N. Narashimhan, "Hydrologic Mechanisms Governing Fluid Flow in a Partially Saturated, Fractured, Porous Medium", Water Resources Res., 21, 12, 1861-74, December, (1985).

7. M.J. Nicholl, R.J. Glass, and H.A. Nguyen, "Gravity-Driven Fingering in Unsaturated Fractures", Proceedings of the Third Annual International Conference on High Level Radioactive Waste Management, Las Vegas, Nevada, April 12-16, (1992).

8. R.J. Glass, "Modeling Gravity-Driven Fingering Using Modified Percolation Theory", Proceedings of the Fourth Annual International Conference on High Level Radioactive Waste Management, Las Vegas, Nevada, April 26-30, (1993).

9. R.J. Glass, and D.L. Norton, "Wetted Region Structure in Horizontal Unsaturated Fractures: Water Entry Through the Surrounding Porous Matrix", Proceedings of the Third Annual International Conference on High Level Radioactive Waste Management, Las Vegas, Nevada, April 12-16, (1992).

10. R.B. Bird, W.E. Stewart, and E.N. Lightfoot, "Transport Phenomena", John Wiley and Sons, NY, (1960).

11. S.R. Brown, "Fluid Flow Through Rock Joints: The Effect of Surface Roughness", J. Geophysical Research, 92, B2, 1337-1347, February, (1987).

12. W.R. Rossen, and A.T.A Kumar, "Single and Two-Phase Flow in Natural Fractures", Proceedings of the 67th Annual Conference and Exhibition, Society Petr. Engrs., 595-603, Wash. DC, October 4-7, (1992).

13. L.J. Pyrak-Nolte, N.G.W. Cook, and D.D. Nolte, "Fluid Percolation Through Single Fractures", Geophysical Res. Letters, 15, 11, 1247-1250, October, (1988).

14. M.J. Nicholl, R.J. Glass, and H.A. Nguyen, "Wetting Front Instability in an Initially Wet Unsaturated Fracture", Proceedings of the Fourth Annual International Conference on High Level Radioactive Waste Management, Las Vegas, Nevada, April 26-30, (1993).

15. L. Smith, and F.W. Schwartz, "Mass Transport 3. Role of Hydraulic Conductivity Data on Prediction", Water Resources Res., vol. 17, no. 5, 1463-1479, October (1981).

16. T.-C.J. Yeh, "Stochastic Modeling of Groundwater Flow and Solute Transport in Aquifers", Hydrological Processes, HYPRE3, 6, 4, 369-395, Oct.-Dec., (1992).